

## Homogenization of fiber-reinforced composites with random properties using the weighted least squares response function approach

M. KAMIŃSKI

*Department of Structural Mechanics  
Faculty of Civil Engineering, Architecture and Environmental Engineering  
Technical University of Łódź  
Al. Politechniki 6, 90-924 Łódź, Poland  
e-mail: Marcin.Kaminski@p.lodz.pl*

THE MAIN AIM OF THE PAPER is a determination of the basic probabilistic characteristics for the effective elasticity tensor of the periodic fiber-reinforced composites, using the generalized stochastic perturbation technique. An evaluation of the generalized stochastic perturbation method of the analytical formulas and the Monte-Carlo simulation technique is provided for the 1D periodic structure with random material parameters. The higher-order terms are determined using numerical determination of the response functions between the effective tensor components and the given random input variables. It is carried out with the use of the Least Squares Method (LSM), applied for the series of computational experiments consisting of the Finite Element Method (FEM) solutions to the cell problems for the randomized input parameters. The key problem is the weighting LSM procedure worked out to speed up the probabilistic convergence of the homogenization results.

**Key words:** homogenization method, random composites, stochastic perturbation method, response function approach, weighted least squares technique.

Copyright © 2011 by IPPT PAN

### 1. Introduction

HOMOGENIZATION METHOD INCLUDING random material properties of the constituents is still a very interesting and extensively studied mathematical and computational problem [6, 7]. It is solved using various strategies – from the classical Monte-Carlo simulation [4, 9], through various orders of stochastic perturbation methods (implemented as the Stochastic Finite Element Method – SFEM) [8, 13], up to some spectral approaches based on the Karhunen–Loeve expansions of the state variables and composite responses [16]. At the same time, a variety of homogenization approaches is also developed, related also to the coupled problems, multiscale heterogeneous structures as well as to the mixtures of solids, fluids and gases [3]. The common point of those two essentially different areas is the perturbation theory, which may serve for both expansion of the macro

responses versus the micro ones in the cell problems (with deterministic coefficients). We engage it also to provide a representation of the input and output random functions, using Taylor series around their expectations (with random coefficients, however). This is the main reason to still develop and make the stochastic perturbation based on the effective modules method more efficient in homogenization of the periodic composites with random material characteristics.

It is known that the general random composite model is based on the assumption that only the mean value of the composite response is the same in each RVE. Usually it follows the fact that periodicity in such a composite is considered as the periodicity of the expected values of some parameters only (like material properties, for instance); higher order statistics are usually assumed to be as unperiodic. More restrictive model is proposed and used below, where the geometry is deterministic and perfectly periodic (fibers' location, radius as well as fiber-matrix interface), while material characteristics are defined as random variables having truncated Gaussian distributions with arbitrarily given first two probabilistic moments. Those moments are identical in each cell (containing a single fiber), so that computational probabilistic homogenization of this cell returns a sufficient statistical information about the entire structure. This approach follows directly some practical applications like the superconducting strands [10], where four components have perfectly periodic distribution in the transversal cross-section and where statistical parameters of material characteristics, as well as the ultimate strength, are provided by the manufacturers. This approach also has an experimental and digital image analysis-based justification, at least for some specific composites [15]. The basic difference between two perturbation-based expansions is also in the additional parameters – spatial representation undergoes with perturbation parameter  $\zeta \rightarrow 0$  (being a decisive limitation of this theory for small number of the periodicity cells in one or even two directions). The second expansion is carried out with the perturbation parameter in random expansion given as  $\varepsilon = 1$ ; in both cases the expansions are analytic with respect to  $\zeta$  and  $\varepsilon$ .

The additional analytical forms are available thanks to the mathematical model of 1D composite in the first case and, in the second case, thanks to the application of the computer algebra system determining the probabilistic moments. The probabilistic expansion is also non-standard, since partial derivatives of the homogenized tensors demanded in the Taylor expansions are calculated analytically, using their least squares approximations with respect to material parameters of the composite constituents. Validation of the generalized stochastic perturbation method with respect to the straightforward integral numerical determination of the probabilistic moments, as well as to the classical Monte-Carlo simulation method, is provided in the case of unidirectional multicomponent structure, where some algebraic expressions for the homogenized tensor are known.

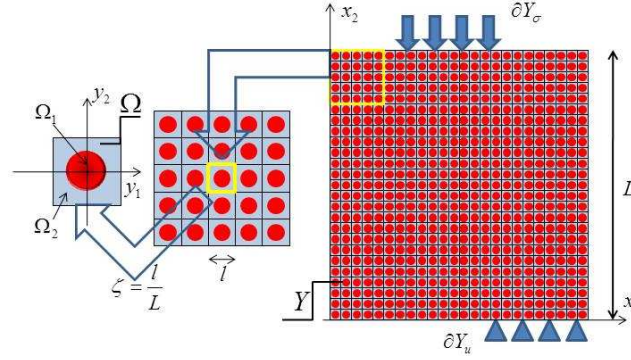
Since general analytical solution to the cell problem is not available in 2D, computational analysis used to determine the probabilistic moments of the homogenized elasticity tensor has a hybrid character. First part is carried out using the Finite Element Method and homogenization-oriented program, whose results are transferred into the computer algebra system to combine several deterministic results into the analytical approximation of the homogenized tensor components. It is done for all input random variables separately and enables final determination of probabilistic characteristics for  $C_{ijkl}^{(\text{eff})}$ . Let us underline that this methodology was applied previously with respect to this particular composite case study, using the Unweighted Least Squares Method (ULSM) to compute the higher order probabilistic perturbations. Probabilistic convergence of the combined ULSM-SFEM is not fast enough, especially for larger random dispersions of the input random parameters, where the differences between the neighboring orders approach zero rather slowly. It may significantly affect the computational cost of the entire simulation and makes it closer to the Monte-Carlo based estimations. As it is known from the numerical analysis developments, the easiest way to overcome this inaccuracy is to apply the Weighted version of the Least Squares Method (WLSM), where various weights are applied to distinguish (in computational aspect) between the trial points lying close enough and rather far away from the additional expected values. Both ULSM and WLSM (in two different versions) are compared below to demonstrate how it is possible to increase efficiency of this hybrid SFEM probabilistic homogenization method and to eliminate the well-known limitation on the stochastic perturbation technique to the relatively small random dispersions. The main benefit of this new procedure is an apparent stabilization of the higher-order perturbations by the user-dependent weights distribution modification. This is also the right way to implement the other than Gaussian probabilistic distributions, also in the context of discrete sets of experimental data smoothed to some analytical probability density functions.

## 2. Homogenization method

### 2.1. General model for a 2D structure

Let us introduce a geometrical scaling parameter  $\zeta > 0$  between the micro- and macroscale of the composite (see Fig. 1), and introduce two coordinate systems:  $\mathbf{y} = (y_1, y_2, y_3)$  on the microscale of the composite and  $\mathbf{x} = (x_1, x_2, x_3)$  on the macroscale.

Let us denote the fiber region by  $\Omega_1$ , the matrix area by  $\Omega_2$  and the interface between them by  $\Gamma_{12}$  (continuous and smooth plane contour). Then, the Representative Volume Element (RVE) denoted further by  $\Omega$ , consists of the

FIG. 1. Periodic composite structure  $Y$ .

single fiber with circular cross-section surrounded by the matrix and centrally located in the square with the length  $l$ . The entire composite structure built up with the net of periodically distributed parallel fibers is denoted here by  $Y$ . As far as the randomness in the fibers' position is taken into account, the Representative Volume Element must contain the few fibers with the pattern or random distribution representative for the entire composite cross-section. Material characteristics of both components – Young's moduli and Poisson's ratios – are defined as the Gaussian random variables truncated to the physically admissible values  $E(\mathbf{y}; \omega) = \{e_1(\omega), e_2(\omega)\}$  and  $\nu(\mathbf{y}; \omega) = \{\nu_1(\omega), \nu_2(\omega)\}$ , having specified the first two probabilistic moments. Denoting by  $\mu_\alpha(\mathbf{b}(\mathbf{y}; \omega))$  the  $\alpha$ -th central probabilistic moment of the field  $\mathbf{b}(\mathbf{y}; \omega)$ , one may express the required periodicity as

$$(2.1) \quad \mu_\alpha(\mathbf{b}(\mathbf{x}; \omega)) = \mu_\alpha(\mathbf{b}(\mathbf{x} + l; \omega)),$$

where

$$(2.2) \quad \mu_\alpha(\mathbf{b}(\mathbf{y}; \omega)) = \chi_1(\mathbf{y})\mu_\alpha(b_1(\omega)) + (1 - \chi_1(\mathbf{y}))\mu_\alpha(b_2(\omega)),$$

with  $\chi_1(\mathbf{y})$  being a characteristic function for the fiber

$$(2.3) \quad \chi_1(\mathbf{y}) = \begin{cases} 1, & \mathbf{y} \in \Omega_1, \\ 0, & \mathbf{y} \in \Omega_2. \end{cases}$$

The problem is to determine the probabilistic moments of the homogenized tensor  $\mu_\alpha(C_{ijkl}^{\text{eff}})$ ,  $\alpha \in \mathbb{N}$ , and it is provided using the extension of the effective modules method available for the deterministically defined periodic composites. The homogenization method described below is not restricted neither to the RVE with the single fiber nor the RVEs with the few fibers of perfectly deterministic geometry. Let us express any state function  $G$  defined on  $Y$  as

$$(2.4) \quad G^\zeta(\mathbf{x}) = G\left(\frac{\mathbf{x}}{\zeta}\right) = G(\mathbf{y}).$$

The linear elasticity problem for the periodic composite structure is given as follows [2, 14]:

$$(2.5) \quad \begin{cases} \frac{\partial \sigma_{ij}^\zeta}{\partial x_j} + F_i = 0, \\ \sigma_{ij}^\zeta n_j = p_i, & \mathbf{x} \in \partial Y_\sigma, \\ u_i^\zeta = 0, & \mathbf{x} \in \partial Y_u, \\ \sigma_{ij}^\zeta = C_{ijkl}^\zeta \varepsilon_{kl}^\zeta, \\ \varepsilon_{kl}^\zeta = \frac{1}{2}(u_{k,l}^\zeta + u_{l,k}^\zeta), \end{cases} \quad i, j, k, l = 1, 2,$$

where  $F_i$  denotes the vector of the external loadings applied on the entire composite structure  $Y$  (most frequently its weight). Assuming a perfect interface between the matrix and the fibers as well as no cracks and other defects in these constituents, we solve this problem by introducing the bilinear form  $a^\zeta(\mathbf{u}, \mathbf{v})$  in the microscale of the composite

$$(2.6) \quad a^\zeta(\mathbf{u}, \mathbf{v}) = \int_{\Omega} C_{ijkl} \left( \frac{\mathbf{x}}{\zeta} \right) \varepsilon_{ij}(\mathbf{u}) \varepsilon_{kl}(\mathbf{v}) d\Omega$$

and the linear one

$$(2.7) \quad L(\mathbf{v}) = \int_{\Omega} F_i v_i d\Omega + \int_{\partial \Omega_\sigma} p_i v_i d(\partial \Omega),$$

in the following Hilbert space of admissible displacements defined on  $Y$ :

$$(2.8) \quad V = \{ \mathbf{v}, \mathbf{v} \in (H^1(Y))^2, \mathbf{v}|_{\partial \Omega_u} = 0 \}, \quad \|\mathbf{v}\|^2 = \int_{\Omega} \varepsilon_{ij}(\mathbf{v}) \varepsilon_{ij}(\mathbf{v}) d\Omega.$$

Then, the variational statement equivalent to the equilibrium problem (2.5) is to find  $\mathbf{u}^\zeta \in V$  being a solution of the following equation:

$$(2.9) \quad a^\zeta(\mathbf{u}^\zeta, \mathbf{v}) = L(\mathbf{v}), \quad \mathbf{v} \in V$$

for any  $\mathbf{u}, \mathbf{v} \in P(\Omega)$ , and for the additional space of the admissible displacement functions  $P(\Omega) = \{ \mathbf{v}, \mathbf{v} \in (H^1(\Omega))^2 \}$ . The homogenization function  $\chi_{(ij)k} \in P(\Omega)$  is a solution to the local problem

$$(2.10) \quad a^\zeta((\chi_{(ij)k} + y_j \delta_{ki}) \mathbf{n}_k, \mathbf{w}) = 0$$

for any  $\mathbf{w} \in P(\Omega)$ , where  $\mathbf{n}_k$  is the additional versor. Assuming further boundedness, ellipticity and symmetry of the elasticity tensor, one may recover the effective elasticity tensor components from the following theorem [2, 14].

The solution  $\mathbf{u}^\zeta$  of problem (2.10) converges weakly in space  $V$

$$(2.11) \quad \mathbf{u}^\zeta \rightarrow \mathbf{u} \quad \text{as} \quad \zeta \rightarrow 0$$

for  $\Omega$ -periodic tensor  $C_{ijkl}^\zeta(\mathbf{y})$ , where the solution  $\mathbf{u}$  is the unique one for the problem

$$(2.12) \quad \mathbf{u} \in V, \quad S(\mathbf{u}, \mathbf{v}) = L(\mathbf{v})$$

for any  $\mathbf{v} \in V$  and

$$(2.13) \quad S(\mathbf{u}, \mathbf{v}) = \int_{\Omega} S_{ijkl} \varepsilon_{ij}(\mathbf{u}) \varepsilon_{kl}(\mathbf{v}) d\Omega,$$

where

$$(2.14) \quad S_{ijkl} = \frac{1}{|\Omega|} a_y((\chi_{(ij)p} + y_i \delta_{pj}) \mathbf{n}_p, (\chi_{(kl)r} + y_l \delta_{rk}) \mathbf{n}_r).$$

It is well known, that the local problem for 2D and 3D structures consists in numerical determination of the homogenization function  $\chi_{(kl)i}$  periodic on  $\Omega$ , satisfying the given equilibrium equations and the following boundary conditions:

$$(2.15) \quad \sigma_{ij}(\mathbf{X}_{(pq)}) n_j = [C_{pqij}]|_{\Gamma_{12}} n_j = C_{pqij}^{(2)} - C_{pqij}^{(1)} \quad \text{on} \quad \Gamma_{12}.$$

Hence, the variational formulation necessary for the displacement version of the Finite Element Method analysis of the local problem can be written out as

$$(2.16) \quad C_{ijkl}^{(1)} \int_{\Omega_1} \varepsilon_{kl}(\mathbf{X}_{(pq)}) \varepsilon_{ij}(\mathbf{v}) d\Omega + C_{ijkl}^{(2)} \int_{\Omega_2} \varepsilon_{kl}(\mathbf{X}_{(pq)}) \varepsilon_{ij}(\mathbf{v}) d\Omega \\ = - \int_{\Gamma_{12}} \sigma_{ij}(\mathbf{X}_{(pq)}) n_j v_i d\Gamma.$$

Finally, one computes the effective elasticity tensor after solving for  $\chi_{(pq)i}$  as

$$(2.17) \quad C_{ijpq}^{(\text{eff})} = \frac{1}{|\Omega|} \int_{\Omega} (C_{ijpq} + C_{ijkl} \varepsilon_{pq}(\mathbf{X}_{(kl)})) d\Omega.$$

Further, it is clear that if the second component of the R.H.S. integrand function is omitted, well-known upper bounds for the effective elasticity tensor for

the composite are returned. The experimental and computational analyses prove that these bounds are easy to be calculated even in the case of random spaces of composite constituents elastic characteristics, but their values significantly overestimate the real effective properties. Let us finally note that since probabilistic method uses the several deterministic solutions to complete the entire homogenization of a random composite, this mathematical apparatus does not need further improvement and the homogenization theorem remains valid.

**2.2. 1D-periodic structure as the special case**

We consider a special case of the multi-component unidirectional composite beam with the prismatic cross-section constant along the beam length, which has perfectly periodic structure [11] and material properties varying along the spatial macro-coordinate  $x_3$  (constant with respect to the remaining axes). Now, the RVE consists of the few layers with deterministically defined thicknesses corresponding to the composite constituents and having perfect interfaces perpendicular to  $x_3$ . The following system of partial differential equations is employed to calculate the effective properties:

$$(2.18) \quad \left( C_{ijkl} \left( \frac{x_3}{\zeta} \right) u_{k,l}^\zeta \right)_{,j} = f_i(\mathbf{x}), \quad \mathbf{u}^\zeta(\mathbf{x}) = \mathbf{u}^o(\mathbf{x}), \quad x \in \partial\Omega.$$

Similarly to the procedure displayed above, the periodic homogenization functions  $\chi_{(mn)}(\mathbf{y})$  are employed and determined as the solution to the local problem on the RVE

$$(2.19) \quad \frac{\partial}{\partial y_j} \left( C_{ijkl}(y_3) \frac{\partial}{\partial y_l} (\chi_{(mn)k}) + C_{ijmn}(y_3) \right) = 0.$$

Obviously, a solution is expected in the form  $\chi_{(mn)}(\mathbf{y}) = \chi_{(mn)}(y_3)$ . It yields

$$(2.20) \quad \frac{\partial}{\partial y_3} \left( C_{i3k3}(y_3) \frac{\partial}{\partial y_3} (\chi_{(mn)k}) + C_{i3mn}(y_3) \right) = 0$$

for any periodic  $\chi_{(mn)}(y_3)$ . Therefore, Eq. (2.20) is transformed into the form

$$(2.21) \quad C_{i3k3}(y_3) \chi_{(mn)k,3} + C_{i3mn}(y_3) = A_i$$

and may be solved explicitly, so that

$$(2.22) \quad \chi_{(mn)k,3} = -\{C_{k3j3}\}^{-1} C_{j3mn} + \{C_{k3j3}\}^{-1} A_j.$$

One obtains from the periodicity condition  $\langle \chi_{(mn),3} \rangle_\Omega = 0$  the result

$$(2.23) \quad 0 = -\langle \{C_{k3j3}\}^{-1} C_{j3mn} \rangle_\Omega + \langle \{C_{k3j3}\}^{-1} \rangle_\Omega A_j.$$

Therefore

$$(2.24) \quad A_i = \langle \{C_{i3k3}\}^{-1} \rangle_{\Omega}^{-1} \langle \{C_{k3j3}\}^{-1} C_{j3mn} \rangle_{\Omega},$$

and there holds

$$(2.25) \quad \begin{aligned} \chi_{(mn)k,3} = & -\{C_{k3j3}\}^{-1} C_{j3mn} \\ & + \{C_{k3j3}\}^{-1} \langle \{C_{j3q3}\}^{-1} \rangle_{\Omega}^{-1} \langle \{C_{q3p3}\}^{-1} C_{p3mn} \rangle_{\Omega}. \end{aligned}$$

Taking into account that the state functions depend only on the  $y_3$  axis, there holds

$$(2.26) \quad C_{ijkl}^{(\text{eff})} = \langle C_{ijkl} + C_{ijm3} \chi_{(kl)m,3} \rangle_{\Omega}.$$

Finally, the homogenized elasticity tensor components are given by

$$(2.27) \quad \begin{aligned} C_{ijkl}^{(\text{eff})} = & \langle C_{ijkl} \rangle_{\Omega} - \langle C_{ijm3} \{C_{m3p3}\}^{-1} C_{p3kl} \rangle_{\Omega} \\ & + \langle C_{ijm3} \{C_{m3p3}\}^{-1} \rangle_{\Omega} \langle \{C_{p3n3}\}^{-1} \rangle_{\Omega}^{-1} \langle \{C_{n3q3}\}^{-1} C_{q3kl} \rangle_{\Omega}. \end{aligned}$$

In case of isotropic and linear elastic constituent materials of this composite, it is obtained after some algebraic manipulation [11]:

$$(2.28) \quad \begin{aligned} C_{1111}^{(\text{eff})} = & C_{2222}^{(\text{eff})} \\ = & \left\langle \frac{(1-\nu)e}{(1+\nu)(1-2\nu)} \right\rangle_{\Omega} - \left\langle \frac{e(1-2\nu)}{1-\nu^2} \right\rangle_{\Omega} + \frac{\langle \frac{1-2\nu}{1-\nu} \rangle_{\Omega}^2}{\langle \frac{(1+\nu)(1-2\nu)}{(1-\nu)e} \rangle_{\Omega}}, \end{aligned}$$

$$(2.29) \quad C_{3333}^{(\text{eff})} = \left\langle \frac{(1+\nu)(1-2\nu)}{(1-\nu)e} \right\rangle_{\Omega}^{-1},$$

$$(2.30) \quad C_{1133}^{(\text{eff})} = C_{3311}^{(\text{eff})} = C_{2233}^{(\text{eff})} = C_{3322}^{(\text{eff})} = \frac{\langle \frac{1-2\nu}{1-\nu} \rangle_{\Omega}}{\langle \frac{(1+\nu)(1-2\nu)}{(1-\nu)e} \rangle_{\Omega}},$$

$$(2.31) \quad C_{1122}^{(\text{eff})} = C_{2211}^{(\text{eff})} = \left\langle \frac{e}{1-\nu} \right\rangle_{\Omega} - \left\langle \frac{e(1-2\nu)}{1-\nu^2} \right\rangle_{\Omega} + \frac{\langle \frac{1-2\nu}{1-\nu} \rangle_{\Omega}}{\langle \frac{(1+\nu)(1-2\nu)}{(1-\nu)e} \rangle_{\Omega}},$$

$$(2.32) \quad C_{1212}^{(\text{eff})} = C_{2121}^{(\text{eff})} = \left\langle \frac{e}{1+\nu} \right\rangle_{\Omega},$$

$$(2.33) \quad C_{1313}^{(\text{eff})} = C_{3131}^{(\text{eff})} = C_{2323}^{(\text{eff})} = C_{3232}^{(\text{eff})} = \left\langle \frac{1}{\frac{1+\nu}{e}} \right\rangle_{\Omega},$$

with the remaining components of the effective elasticity tensor equal to 0. The equations given above enable both the analytical derivations of the probabilistic moments for the given random variable in the system, the Monte-Carlo simulation of the homogenized tensor and the generalized stochastic-perturbation based computational analysis; all those techniques are discussed in Section 5.1.

### 3. Generalized stochastic perturbation technique in homogenization

The probabilistic perturbation methodology is proposed to calculate the moments of the homogenized elasticity tensor discussed above. It is based on an expansion via the Taylor series about the spatial expectations using a small parameter  $\varepsilon > 0$  and the following expression is employed for the effective tensor components [8]:

$$(3.1) \quad C_{ijkl}^{(\text{eff})}(b) = C_{ijkl}^{(\text{eff})0} + \varepsilon \frac{\partial C_{ijkl}^{(\text{eff})}}{\partial b} \Delta b + \frac{1}{2} \varepsilon^2 \frac{\partial^2 C_{ijkl}^{(\text{eff})}}{\partial b^2} (\Delta b)^2 + \dots \\ + \frac{1}{n!} \varepsilon^n \frac{\partial^n C_{ijkl}^{(\text{eff})}}{\partial b^n} (\Delta b)^n,$$

where  $b$  stands for the random input,  $\Delta b$  denotes the variation of this variable around its expected value; the accuracy of this expansion strongly depends on the perturbation order  $n$ . The recursive formula for the central  $m$ -th order probabilistic moment in the 10-th order approximation, can be determined as [1, 7]

$$(3.2) \quad \mu_m(C_{ijkl}^{(\text{eff})}(b)) \\ = \int_{-\infty}^{+\infty} \left( C_{ijkl}^{(\text{eff})0}(b) + \sum_{i=1}^n \frac{\varepsilon^i}{i!} \Delta b^i \frac{\partial^i C_{ijkl}^{(\text{eff})}(b)}{\partial b^i} - E[C_{ijkl}^{(\text{eff})}(b)] \right)^m p(b) db \\ = \int_{-\infty}^{+\infty} \left( \varepsilon \frac{\partial C_{ijkl}^{(\text{eff})}(b)}{\partial b} \Delta b + \dots + \frac{\varepsilon^{10}}{10!} \frac{\partial^{10} C_{ijkl}^{(\text{eff})}(b)}{\partial b^{10}} (\Delta b)^{10} \right)^m p(b) db.$$

Then, the expected value and the variance of the resulting homogenized tensor  $C_{ijkl}^{(\text{eff})}(b)$  can be obtained for the Gaussian input parameter  $b$  as

$$(3.3) \quad E[C_{ijkl}^{(\text{eff})}] = C_{ijkl}^{(\text{eff})0}(b) + \frac{1}{2} \frac{\partial^2 C_{ijkl}^{(\text{eff})}(b)}{\partial b^2} \text{Var}(b) \\ + \frac{1}{4!} \frac{\partial^4 C_{ijkl}^{(\text{eff})}(b)}{\partial b^4} \mu_4(b) + \frac{1}{6!} \frac{\partial^6 C_{ijkl}^{(\text{eff})}(b)}{\partial b^6} \mu_6(b) + \dots \\ + \frac{1}{2m!} \frac{\partial^{2m} C_{ijkl}^{(\text{eff})}(b)}{\partial b^{2m}} \mu_{2m}(b) \\ = C_{ijkl}^{(\text{eff})0}(b) + \frac{1}{2} C_{ijkl}^{(\text{eff})(2)}(b) + \frac{1}{4!} C_{ijkl}^{(\text{eff})(4)}(b) + \frac{1}{6!} C_{ijkl}^{(\text{eff})(6)}(b) + \dots \\ + \frac{1}{2m!} C_{ijkl}^{(\text{eff})(2m)}(b)$$

and, furthermore,

$$\begin{aligned}
 (3.4) \quad \text{Var}(C_{ijkl}^{(\text{eff})}) &= \text{Var}(b) \frac{\partial C_{ijkl}^{(\text{eff})}}{\partial b} \frac{\partial C_{ijkl}^{(\text{eff})}}{\partial b} \\
 &+ \mu_4(b) \left( \frac{1}{4} \frac{\partial^2 C_{ijkl}^{(\text{eff})}}{\partial b^2} \frac{\partial^2 C_{ijkl}^{(\text{eff})}}{\partial b^2} + \frac{2}{3!} \frac{\partial C_{ijkl}^{(\text{eff})}}{\partial b} \frac{\partial^3 C_{ijkl}^{(\text{eff})}}{\partial b^3} \right) \\
 &+ \mu_6(b) \left( \left( \frac{1}{3!} \right)^2 \frac{\partial^3 C_{ijkl}^{(\text{eff})}}{\partial b^3} \frac{\partial^3 C_{ijkl}^{(\text{eff})}}{\partial b^3} + \frac{1}{4!} \frac{\partial^4 C_{ijkl}^{(\text{eff})}}{\partial b^4} \frac{\partial^2 C_{ijkl}^{(\text{eff})}}{\partial b^2} \right. \\
 &\left. + \frac{2}{5!} \frac{\partial^5 C_{ijkl}^{(\text{eff})}}{\partial b^5} \frac{\partial C_{ijkl}^{(\text{eff})}}{\partial b} \right) + \dots,
 \end{aligned}$$

where  $\mu_k(b)$  is the  $k$ -th central probabilistic moment of the variable  $b$ . The perturbation parameter is adopted as  $\varepsilon = 1$  and only the first few perturbations are included, especially in the last relation. Quite similarly, using the first and the second order terms only, it is possible to derive the third order probabilistic moments as

$$\begin{aligned}
 (3.5) \quad \mu_3(C_{ijkl}^{(\text{eff})}(b)) &= \int_{-\infty}^{+\infty} (C_{ijkl}^{(\text{eff})})^0 + \frac{\partial C_{ijkl}^{(\text{eff})}}{\partial b} \Delta b + \frac{1}{2} \frac{\partial^2 C_{ijkl}^{(\text{eff})}}{\partial b^2} (\Delta b)^2 + \dots \\
 &\quad - E[C_{ijkl}^{(\text{eff})}(b)]^3 p(b) db \\
 &\cong \frac{3}{2} \mu_4(b) \left( \frac{\partial C_{ijkl}^{(\text{eff})}}{\partial b} \right)^2 \frac{\partial^2 C_{ijkl}^{(\text{eff})}}{\partial b^2} + \frac{1}{8} \mu_6(b) \left( \frac{\partial^2 C_{ijkl}^{(\text{eff})}}{\partial b^2} \right)^3,
 \end{aligned}$$

and also the fourth order probabilistic moment

$$\begin{aligned}
 (3.6) \quad \mu_4(C_{ijkl}^{(\text{eff})}(b)) &= \int_{-\infty}^{+\infty} (C_{ijkl}^{(\text{eff})})^0 + \frac{\partial C_{ijkl}^{(\text{eff})}}{\partial b} \Delta b + \frac{1}{2} \frac{\partial^2 C_{ijkl}^{(\text{eff})}}{\partial b^2} (\Delta b)^2 + \dots \\
 &\quad - E[C_{ijkl}^{(\text{eff})}(b)]^4 p(b) db \\
 &\cong \mu_4(b) \left( \frac{\partial C_{ijkl}^{(\text{eff})}}{\partial b} \right)^4 + \frac{3}{2} \mu_6(b) \left( \frac{\partial C_{ijkl}^{(\text{eff})}}{\partial b} \frac{\partial^2 C_{ijkl}^{(\text{eff})}}{\partial b^2} \right)^2 \\
 &\quad + \frac{1}{16} \mu_8(b) \left( \frac{\partial^2 C_{ijkl}^{(\text{eff})}}{\partial b^2} \right)^4.
 \end{aligned}$$

Then, one defines the coefficients of variation, asymmetry and concentration as

$$\begin{aligned}
 \alpha(C_{ijkl}^{(\text{eff})}(b)) &= \frac{\sqrt{\text{Var}(C_{ijkl}^{(\text{eff})})}}{E(C_{ijkl}^{(\text{eff})})}; \\
 \beta(C_{ijkl}^{(\text{eff})}(b)) &= \frac{\mu_3(C_{ijkl}^{(\text{eff})})}{(\sqrt{\text{Var}(C_{ijkl}^{(\text{eff})})})^3}; \\
 \gamma(C_{ijkl}^{(\text{eff})}(b)) &= \frac{\mu_4(C_{ijkl}^{(\text{eff})})}{(\text{Var}(C_{ijkl}^{(\text{eff})}))^2}.
 \end{aligned}
 \tag{3.7}$$

As it can be seen in these equations, the symbolic approach perfectly reflects the needs of higher-order perturbation approaches, where the perturbation parameter  $\varepsilon$  with increasing powers can be inserted directly in the Taylor series expansion; this is implemented in numerical experiments to compute symbolically up to the 10-th order expression. It should be clearly undelined that these equations are still independent from the probability distribution type, except that it must be symmetric. The Gaussian and lognormal distributions are decisively preferred here since recursive formulas for all probabilistic moments may be easily implemented into the symbolic computer programs; otherwise, some extra mathematical transforms or a priori assumptions need to be done – only the distributions having the analytical function generating probabilistic moments are applicable here.

## 4. Computational implementation

### 4.1. Finite element discretization of the homogenization problem

Let us introduce the following approximation of homogenization functions  $\chi_{(uv)i}^\delta$  at any point of the considered continuum  $\Omega$  in terms of a finite number of generalized coordinates  $q_{(uv)\alpha}^\delta$  and shape functions  $\varphi_{i\alpha}$  [7–9]:

$$\chi_{(uv)i}^\delta = \varphi_{i\alpha} q_{(uv)\alpha}^\delta, \quad i, u, v = 1, 2, \quad \alpha = 1, \dots, N, \quad \delta = 1, \dots, M.
 \tag{4.1}$$

The variables  $i, u, v$  stand for the spatial coordinates,  $\alpha$  denotes the degree of freedom, where  $N$  is the total number of degrees of freedom,  $\delta$  denotes the current least squares method test number, where  $M$  is the a priori chosen total number of those tests. We discretize the strain  $\varepsilon_{ij}(\chi_{(uv)k}^\delta)$  as well as stress tensors  $\sigma_{ij}(\chi_{(uv)k}^\delta)$  analogously

$$\varepsilon_{ij}(\mathbf{X}_{(uv)}^\delta) = B_{ij\alpha} q_{(uv)\alpha}^\delta,
 \tag{4.2}$$

$$\sigma_{ij}(\mathbf{X}_{(uv)}^\delta) = \sigma_{ij}(\mathbf{X}_{(uv)}^\delta) = C_{ijkl}^\delta \varepsilon_{kl}(\mathbf{X}_{(uv)}^\delta) = C_{ijkl}^\delta B_{kl\alpha} q_{(uv)\alpha}^\delta,
 \tag{4.3}$$

where  $B_{kl\alpha}$  is the shape functions derivatives matrix, which does not vary on the least squares approximation test. Therefore, the virtual work equation is obtained as

$$(4.4) \quad \int_{\Omega} \delta \chi_{(uv)i,j}^{\delta} C_{ijkl}^{\delta} \chi_{(uv)k,l}^{\delta} d\Omega \\ = - \int_{\Gamma_{12}} \delta \chi_{(uv)i}^{\delta} [F_{(uv)i}^{\delta}]|_{\Gamma_{12}} d\Gamma \quad (\text{no summation on } u, v).$$

The Finite Element Method formulation continues with a definition of the global stiffness matrix given as follows:

$$(4.5) \quad K_{\alpha\beta}^{\delta} = \sum_{e=1}^E K_{\alpha\beta}^{(e)\delta} = \sum_{e=1}^E \int_{\Omega_e} C_{ijkl}^{(e)\delta} B_{ij\alpha} B_{kl\beta} d\Omega.$$

Introduction of this matrix into Eq. (4.4) and minimization of this statement with respect to the generalized coordinates enables to write that

$$(4.6) \quad K_{\alpha\beta}^{\delta} q_{(uv)\beta}^{\delta} = Q_{(uv)\alpha}^{\delta},$$

where the R.H.S. vector consists of the stress interface conditions varying also together with the least squares test. The symmetry conditions on the periodicity cell quarter are assumed, so that the orthogonal displacements for every nodal point belonging to the external boundaries of  $\Omega$  are fixed to compute  $3M$  homogenization functions ( $\chi_{(uv)i}^{\delta}$  for  $\delta = 1, \dots, M$ ) and the resulting homogenizing stress fields. Finally, they are spatially averaged into all finite elements constituting the RVE and combined with the original additional elasticity tensor components according to Eq. (2.17)

$$(4.7) \quad C_{ijpq}^{(\text{eff})\delta} = \frac{1}{|\Omega|} \int_{\Omega} (C_{ijpq}^{\delta} + C_{ijkl}^{\delta} \varepsilon_{pq}(\mathbf{x}_{(kl)}^{\delta})) d\Omega.$$

Moreover, we use the following polynomial representation of the homogenized elasticity tensor and its  $s$ -th order partial derivatives:

$$(4.8) \quad C_{ijkl}^{(\text{eff})} = \sum_{r=1}^n A_{ijkl}^{(r)} b^r + A_{ijkl}^{(0)},$$

$$(4.9) \quad \frac{\partial^s C_{ijkl}^{(\text{eff})}}{\partial b^s} = \begin{cases} \sum_{r=1}^s A_{ijkl}^{(r)} P(r-s+1, s) b^{r-s}, & r \leq s, \\ 0, & r > s, \end{cases}$$

as long as  $n \leq \delta$ , where the coefficients  $A_{ijkl}^{(r)}$  are found using the least squares approximation procedure, and where  $P(r - s + 1, s)$  denotes the Porchhammer symbol introduced usually as

$$(4.10) \quad P(z, n) = z(z + 1)(z + 2) \dots (z + n - 1) = \frac{\Gamma(z + n)}{\Gamma(z)}.$$

The polynomial representation (4.8), as the entire homogenization method, is convenient only for the linear elastic transverse isotropy, but corresponds to any random variables because of its purely numerical character. Computational implementation of the nonlinear constitutive models like the elasto-plastic for instance, neglecting the necessary modifications in the homogenization method itself, may not be so straightforward. The expected values are extracted here as

$$(4.11) \quad \begin{aligned} E[C_{ijkl}^{(\text{eff})}] &= C_{ijkl}^{(\text{eff})0} + \frac{1}{2!} \varepsilon^2 \mu_2(b) \sum_{p=1}^n p(p-1) A_{ijkl}^{(p)} b^{p-2} \\ &+ \frac{1}{4!} \varepsilon^4 \mu_4(b) \sum_{p=1}^n p(p-1)(p-2)(p-3) A_{ijkl}^{(p)} b^{p-4} \\ &+ \frac{1}{6!} \varepsilon^6 \mu_6(b) \sum_{p=1}^n p \dots (p-5) A_{ijkl}^{(p)} b^{p-6} \\ &+ \frac{1}{8!} \varepsilon^8 \mu_8(b) \sum_{p=1}^n p \dots (p-7) A_{ijkl}^{(p)} b^{p-8} \\ &+ \frac{1}{10!} \varepsilon^{10} \mu_{10}(b) \sum_{p=1}^n p \dots (p-9) A_{ijkl}^{(p)} b^{p-10}, \end{aligned}$$

and higher order moments determination proceeds similarly. Finally, we notice that for the randomized material parameters we can apply a semi-analytical approach, where the classical definition

$$(4.12) \quad \begin{aligned} C_{ijpq}^{(\text{eff})} &= \left\langle \delta_{ij} \delta_{pq} \frac{e\nu}{(1 + \nu)(1 + 2\nu)} + (\delta_{ip} \delta_{jq} + \delta_{iq} \delta_{jp}) \frac{e}{2(1 + \nu)} \right\rangle_{\Omega} \\ &+ \langle C_{ijkl} \varepsilon_{pq}(\mathbf{X}_{(kl)}) \rangle_{\Omega} \end{aligned}$$

leads to some further simplifications. The partial derivatives of the first component with respect to the given parameter  $b$  are determined from direct analytical differentiations and the second component needs some least square method approximations.

#### 4.2. Weighted least squares technique for the response functions

Consider a set of  $m$  data points  $(b^{(i)}, C_{\alpha\beta\gamma\delta}^{(\text{eff})^{(i)}})$  for  $\alpha, \beta, \gamma, \delta = 1, 2, 3$ , the nonlinear continuous function  $C_{\alpha\beta\gamma\delta}^{(\text{eff})} = f(b, x)$  and a curve (approximating function)  $C_{\alpha\beta\gamma\delta}^{(\text{eff})} = f(b, A_{\alpha\beta\gamma\delta})$ , which additionally depends on  $n$  parameters  $A_{\alpha\beta\gamma\delta}^{(j)}$ ,  $j = 1, \dots, n$ , where  $m \geq n$ . The basic difference from the traditional least squares technique is the presence of the fourth order tensors, which are the main goal of this approximation procedure. We define the additional residuals (rests)  $r_i(C_{\alpha\beta\gamma\delta}^{(\text{eff})})$  as

$$(4.13) \quad r_{\alpha\beta\gamma\delta(i)} = r_i(C_{\alpha\beta\gamma\delta}^{(\text{eff})}) = C_{\alpha\beta\gamma\delta}^{(\text{eff})^{(i)}} - f(b^{(i)}, A_{\alpha\beta\gamma\delta}^{(i)}),$$

to determine the components of the tensor  $A_{\alpha\beta\gamma\delta}$  from the minimization of the following sum:

$$(4.14) \quad S_{\alpha\beta\gamma\delta} = \sum_{i=1}^m w_{ii} r_{\alpha\beta\gamma\delta(i)}^2, \quad \alpha, \beta, \gamma, \delta = 1, 2.$$

It proceeds using the gradient method, so that

$$(4.15) \quad \frac{\partial S_{\alpha\beta\gamma\delta}}{\partial A_{\alpha\beta\gamma\delta}^{(j)}} = -2 \sum_{i=1}^m w_{ii} r_{\alpha\beta\gamma\delta(i)} \frac{\partial f(b^{(i)}, A_{\alpha\beta\gamma\delta}^{(i)})}{\partial A_{\alpha\beta\gamma\delta}^{(j)}} = 0;$$

$$j = 1, \dots, n; \quad \alpha, \beta, \gamma, \delta = 1, 2.$$

Further, we adopt the following notation:

$$(4.16) \quad D_{ij}^{\alpha\beta\gamma\delta} = \frac{\partial f(b^{(i)}, A_{\alpha\beta\gamma\delta}^{(i)})}{\partial A_{\alpha\beta\gamma\delta}^{(j)}}; \quad j = 1, \dots, n; \quad \alpha, \beta, \gamma, \delta = 1, 2,$$

and we form the modified equations as

$$(4.17) \quad \sum_{i=1}^n \sum_{k=1}^m D_{ij}^{\alpha\beta\gamma\delta} w_{ii} D_{ik}^{\alpha\beta\gamma\delta} \hat{A}_{\alpha\beta\gamma\delta}^{(k)} = \sum_{i=1}^n D_{ij}^{\alpha\beta\gamma\delta} w_{ii} C_{\alpha\beta\gamma\delta}^{(\text{eff})^{(i)}},$$

$$j = 1, \dots, n, \quad \alpha, \beta, \gamma, \delta = 1, 2,$$

having the matrix form

$$(4.18) \quad ((\mathbf{D}^{\alpha\beta\gamma\delta})^T \mathbf{w} \mathbf{D}^{\alpha\beta\gamma\delta}) \mathbf{A}^{\alpha\beta\gamma\delta} = (\mathbf{A}^{\alpha\beta\gamma\delta})^T \mathbf{w} \mathbf{C}_{\alpha\beta\gamma\delta}^{(\text{eff})}.$$

After numerical solution to this equation for  $\mathbf{A}^{\alpha\beta\gamma\delta}$ , the final polynomial approximation given by Eq. (4.8) is obtained; this form of the approximating function is well justified by the numerical experiments performed in the next section. The main aim of the weighting procedure inserted into the least squares approximation for the homogenized tensor components with respect to the input random variable is to speed up the probabilistic convergence for basic random moments and characteristics of this tensor components.

## 5. Computational experiments

### 5.1. Validation of the perturbation method for 1D composite

Computational illustration is provided for the two-component composite with the mean values of elastic parameters  $e_1 = 84$  GPa,  $\nu_1 = 0.22$  (for the reinforcement) and for the matrix taken as  $e_2 = 4$  GPa,  $\nu_2 = 0.34$  (both having the same volume fractions). Now, Young's modulus of the stronger material is taken as the input random variable in numerical simulation, where the standard deviation corresponds to its 10% random dispersion – theoretical probability density function and the simulated counterpart (total number of the random trials equals  $10^5$ ) are shown in Fig. 2. The entire analysis is provided using the symbolic environment of the system MAPLE, v. 13, using the relations (2.28)–(2.33), where:

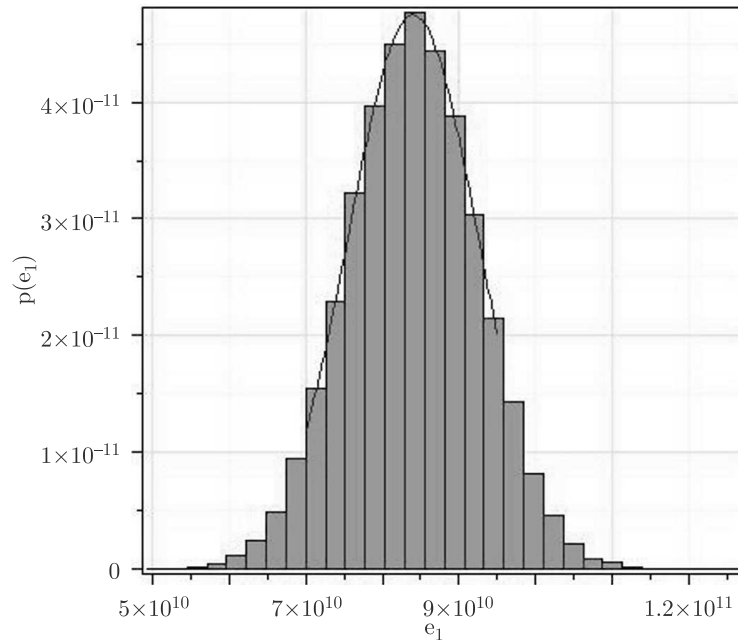


FIG. 2. Initial histogram and theoretical PDF of the reinforcement's Young modulus.

Table 1. A comparison of analytical (AM), statistical (MC) and perturbation-based (PM) probabilistic characteristics of the homogenized tensor.

Probabilistic characteristics	$C_{1111} = C_{2222}$	$C_{3333}$	$C_{1133} = C_{3311}$ $= C_{3322} = C_{2233}$	$C_{1122} = C_{2211}$	$C_{1212} = C_{2121}$	$C_{1313} = C_{3131}$ $= C_{2323} = C_{3232}$
$E[X]$	2.9929E10 (AM) 2.9927E10 (MC) 2.9929E10 (PM)	1.1564E10 1.1564E10 1.1564E10	6.9545E9 6.9545E9 6.9546E9	3.8391E10 3.8389E10 3.8391E10	3.5919E10 3.5916E10 3.5919E10	5.7197E9 5.7197E9 5.7198E9
$\text{Var}(X)$	5.5343E18 (AM) 5.5260E18 (MC) 5.5211E18 (PM)	5.2451E15 5.2453E15 5.0237E15	1.8970E15 1.8971E15 1.8170E15	8.7387E18 8.7414E18 8.7324E18	1.1852E19 1.1855E19 1.1852E19	6.1053E14 6.1054E14 5.8366E14
$\sigma(X)$	2.3504E9 (AM) 2.3507E9 (MC) 2.3497E9 (PM)	7.2423E7 7.2424E7 7.0878E7	4.3555E7 4.3556E7 4.2626E7	2.9561E9 2.9566E9 2.9551E9	3.4426E9 3.4431E9 3.4426E9	2.4709E7 2.4709E7 2.4159E7
$\mu_4(X)$	9.1634E37 (AM) 9.1348E37 (MC) 9.1451E37 (PM)	1.0343E32 1.0260E32 9.0917E31	1.3530E31 1.3421E31 1.1893E31	2.2936E38 2.2864E38 2.2878E38	4.2138E38 4.2008E38 4.2138E38	1.4152E30 1.4035E30 1.2350E30
$\alpha(X)$	0.0785 (AM) 0.0785 (MC) 0.0785 (PM)	0.0063 0.0063 0.0061	0.0063 0.0063 0.0061	0.0770 0.0770 0.0770	0.0958 0.0959 0.0958	0.0043 0.0043 0.0042
$\beta(X)$	-0.0066 (AM) -0.0057 (MC) -0.0094 (PM)	-0.6053 -0.6000 -0.8259	-0.6053 -0.6000 -0.8259	-0.0085 -0.0075 -0.0120	9.0630E-9 8.6663E-4 2.1499E-8	-0.6193 -0.6139 -0.8416
$\kappa(X)$	3.0026 (AM) 2.9915 (MC) 3.0000 (PM)	3.7596 3.7292 3.6024	3.7596 3.7292 3.6024	3.0034 2.9921 3.0001	3.0000 2.9889 3.0000	3.7967 3.7652 3.6254

(a) direct numerical integration following classical definitions of the probability theory, (b) Monte-Carlo simulation and statistical estimation together with (c), the response functions and the generalized stochastic perturbation technique equations are implemented. First strategy needs some attention since general integration in the system MAPLE is unavailable in this case for the unbounded real domain, so that bounded numerical integration is provided within the limits 0 and double expectation. They are found after some a posteriori error-based analysis, where minimization of the computational domain width is carried out with respect to some a priori given error level. The results for all homogenized tensor components are collected in Table 1 below in the form of the expected values (Pa), variances (Pa<sup>2</sup>), standard deviations (Pa), fourth central probabilistic moments (Pa<sup>4</sup>), as well as of the coefficients of variation, skewness and concentration (dimensionless).

The general conclusion is that all the methods return almost the same results – agreement in the expected values as well as in the coefficients of concentration is perfect, some extremely small differences appear for the second-order characteristics, while the largest differences are noticed in case of the skewnesses. The agreement of those techniques mainly follows the fact that the effective tensor components come from the algebraic transformations during smearing of the original materials within the RVE, but the homogenization function has analytical form unlike in most of the 2D problems, where some small differences caused by the SFEM itself are observed. Quite naturally, the largest variations in between those methods are noticed for the homogenized tensor components indexed with ‘3’ since random variable is smeared in this direction together with the deterministic quantity – Young’s modulus of the weaker material. This tensor shows also some probabilistic damping since output coefficients of variations are generally smaller than for the input random variable. Also generally one can conclude that quite independently from the numerical strategy, the effective tensor appears to be Gaussian, since its components have higher order characteristics typical for this distribution. The generalized stochastic perturbation method seems to be efficient, but some further implementation needs to be provided to eliminate the errors in the third order characteristics numerical determination.

## 5.2. Homogenization of the fiber-reinforced structure

Numerical analysis of the periodic random fiber-reinforced composite homogenization is performed using the FEM homogenization-oriented program MCC-EFF and the computer algebra system MAPLE, v. 13. Internal automatic generator in the first program meshes itself the square RVE with centrally located round fiber occupying 34% of the RVE – the mesh consists of 144 4-noded plane

strain finite elements and 153 nodes [7]. Elastic parameters of the fiber material are taken as in the previous computational example; since the Poisson ratio for the matrix has been detected for this composite as the most influential parameter before [7, 8], it is treated now as the truncated Gaussian random variable, where the value given above is its expectation and input coefficient of variation  $\alpha$  is the additional parameter in this study. A discretization of the random variable consists of 11 trial equidistant points, which are symmetrically located around the expectation (the basic length of this subdivision equals 0.01 – about 3% of the mean value); each time the first component of the homogenized elasticity tensor  $C_{1111}^{(\text{eff})}$  is observed. The importance of all the results in the ULSM technique is the same and equals 1, the triangular weights distribution is defined uniquely by the following set  $w_i = [1, 2, 3, 4, 5, 6, 5, 4, 3, 2, 1]$ , while the Dirac-type weights distribution is defined as  $w_i = [1, 1, 1, 1, 1, 6, 1, 1, 1, 1, 1]$ . One can guess that some intermediate nonlinear weights distributions over the trial set have no clear justification, so that those three capabilities are contrasted here. Numerical results from this analysis are shown as the response functions obtained using ULSM technique in Fig. 3 (the entire variability interval of  $\nu_2$ ), in

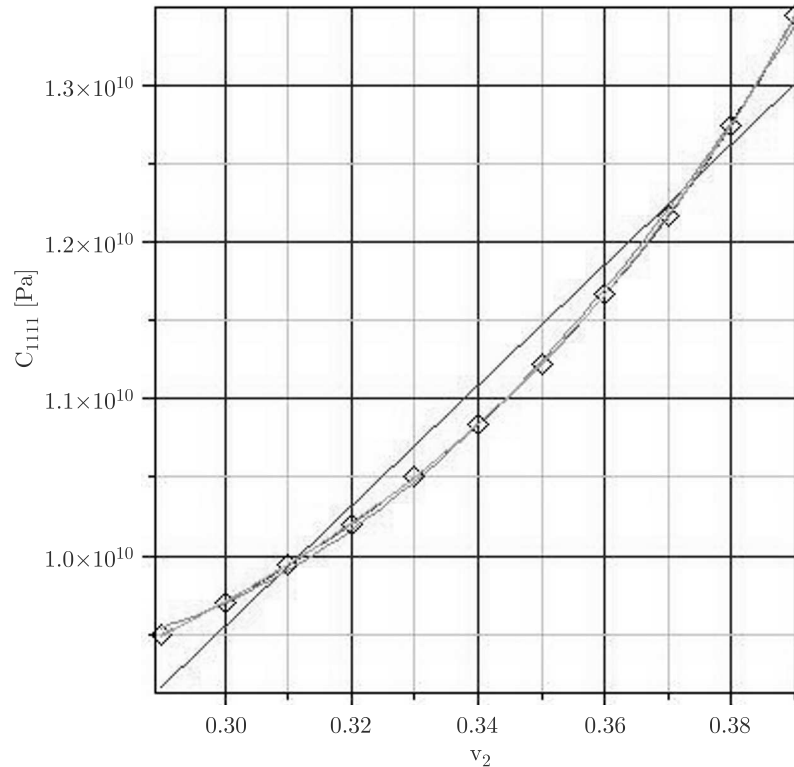


FIG. 3. The ULSM response function  $C_{1111}^{(\text{eff})} = C_{1111}^{(\text{eff})}(\nu_2)$ , wide neighborhood.

Fig. 4 (in the close neighborhood of the expectation), in Fig. 5 – thanks to the WLSM approach for the triangular weights distribution (left-hand diagram) and for the Dirac type distribution (at the right). They are all shown for various response polynomial orders, from 1 to 9, to demonstrate the optimum order of this approximant.

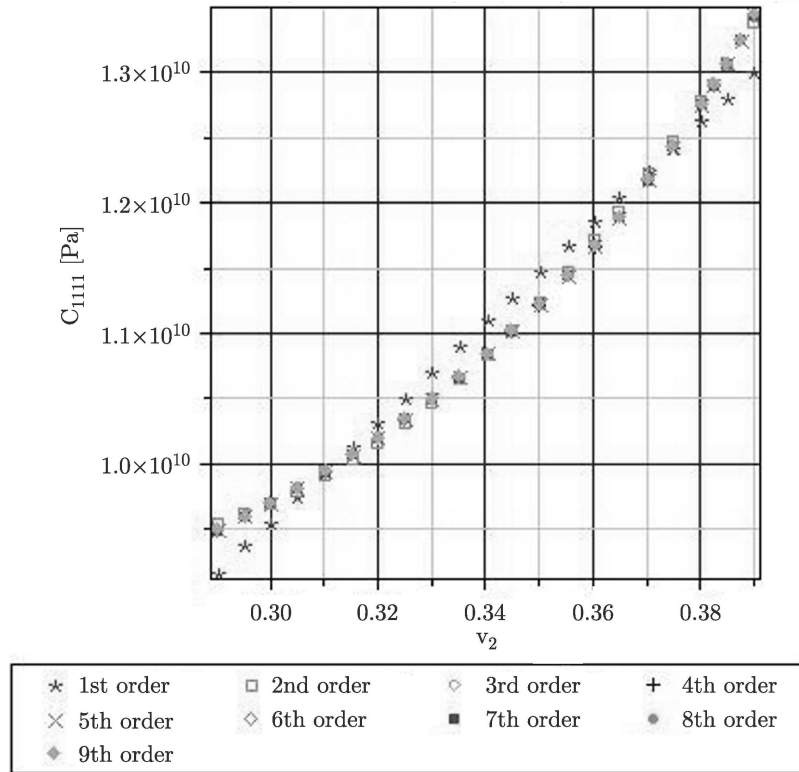


FIG. 4. The ULSM response function  $C_{1111}^{(eff)} = C_{1111}^{(eff)}(\nu_2)$ , close neighborhood.

It is apparent that all order approximations (except for the first one), exhibit really very small differences and it is almost impossible to distinguish between higher-order functions in all approaches (the trial points are marked in Fig. 3 using diamonds – they fit the ULSM approximation perfectly). One may notice that the distance between the first-order approximation and the final function taken at the expectation of input variable, is the largest for the unweighted technique and significantly smaller for the weighted methods. The next set of figures, cf. Figs. 6–7, show essentially different expectations computed and presented as the functions of the input coefficient of variation.

It should be mentioned that determination of those interrelations without the usage of some computer algebra system would be extremely difficult. First of all,

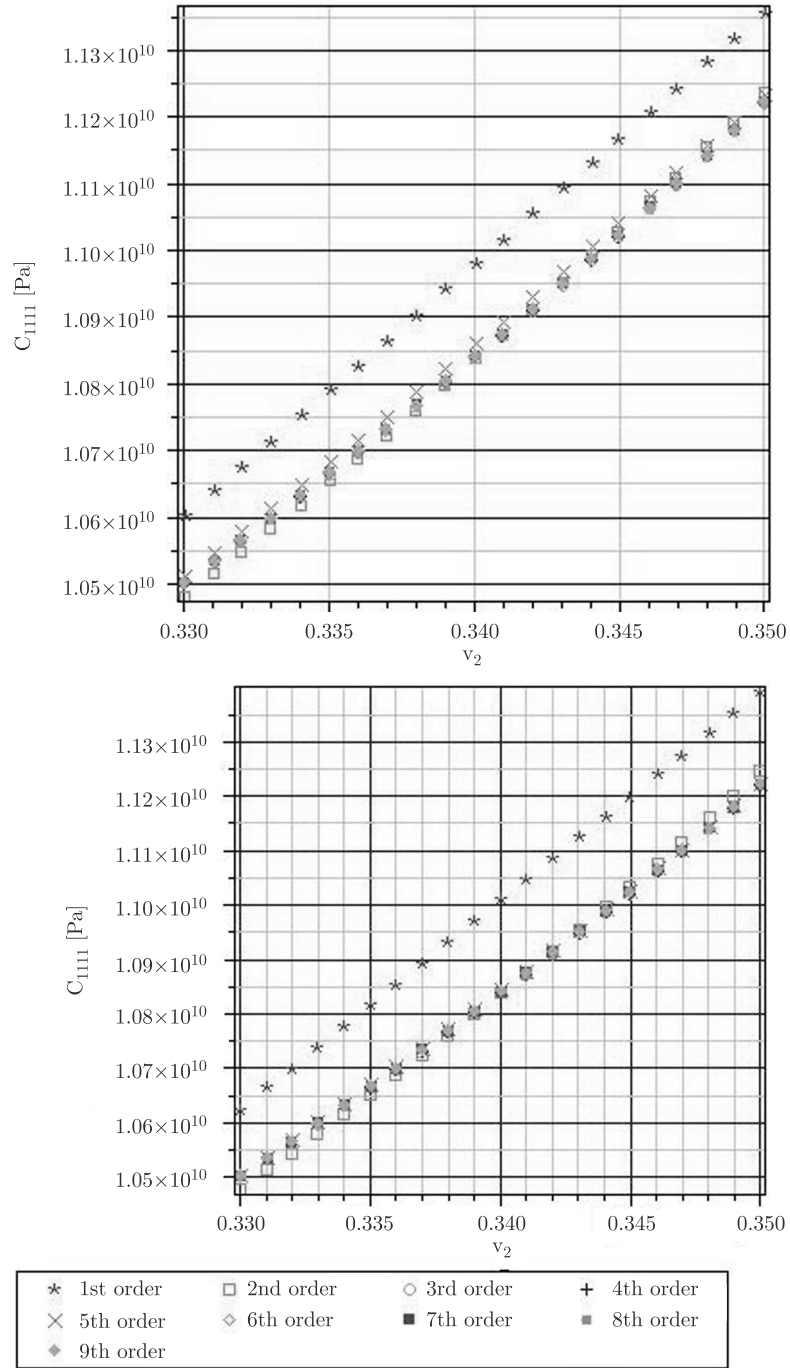


FIG. 5. The WLSM response function  $C_{1111}^{(\text{eff})} = C_{1111}^{(\text{eff})}(\nu_2)$ , triangular vs. Dirac weights.

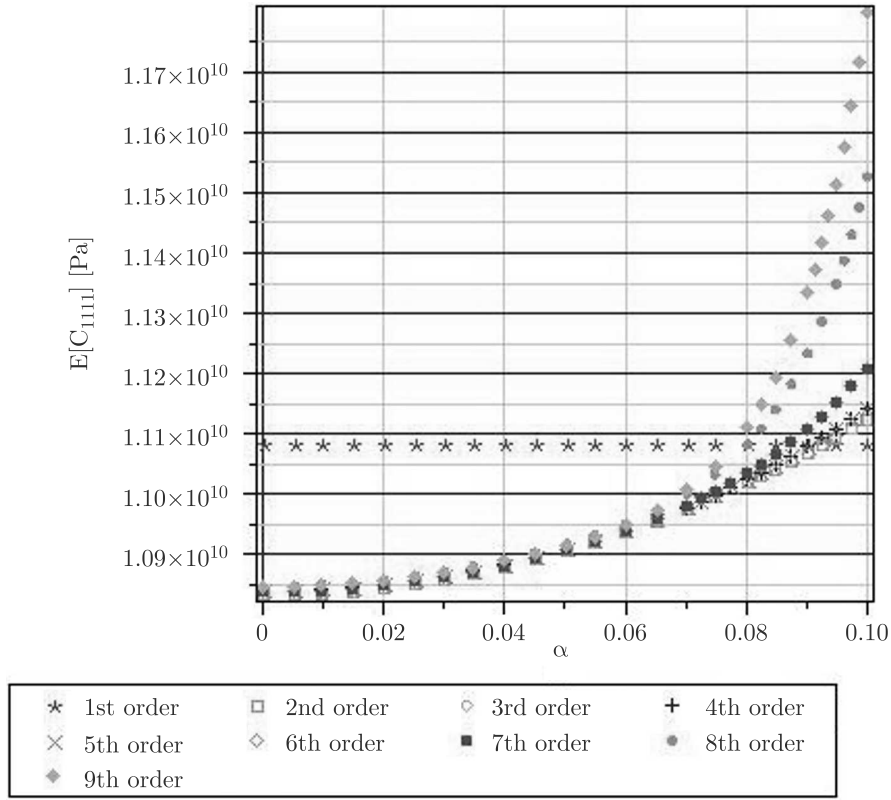


FIG. 6. The ULSM expected values  $E[C_{1111}^{(eff)}(\nu_2)]$ .

the expectations computed even for the first order response polynomial are different for the three models compared, but each time they are quite insensitive to input random dispersion. Obviously, the higher order response functions result each time in the nonlinear, fully convex interrelations between  $E[C_{1111}^{(eff)}]$  and  $\nu_2$ ; apparently, the ULSM appears to be almost divergent for maximum value of the parameter  $\alpha$ , whereas both WLSM approaches show good convergence together with both additional increases of the approximating polynomial and input random dispersion. Comparing carefully left- and right-hand diagrams in Fig. 7, one can see that the application of the Dirac weights definitely eliminates some numerical discrepancies that can be obtained for the middle-order approximants (like the 5-th-order here) – some subtle differences in the response functions weighted using those two types of distributions are found. Finally, the maximum expected values obtained for  $\alpha(\nu_2) = 0.10$  are also different – the largest are computed for ULSM, then for triangular WLSM, and the minimum is detected for Dirac WLSM, so that the conclusion is that the last approach guarantee the most stable results for the expectations.

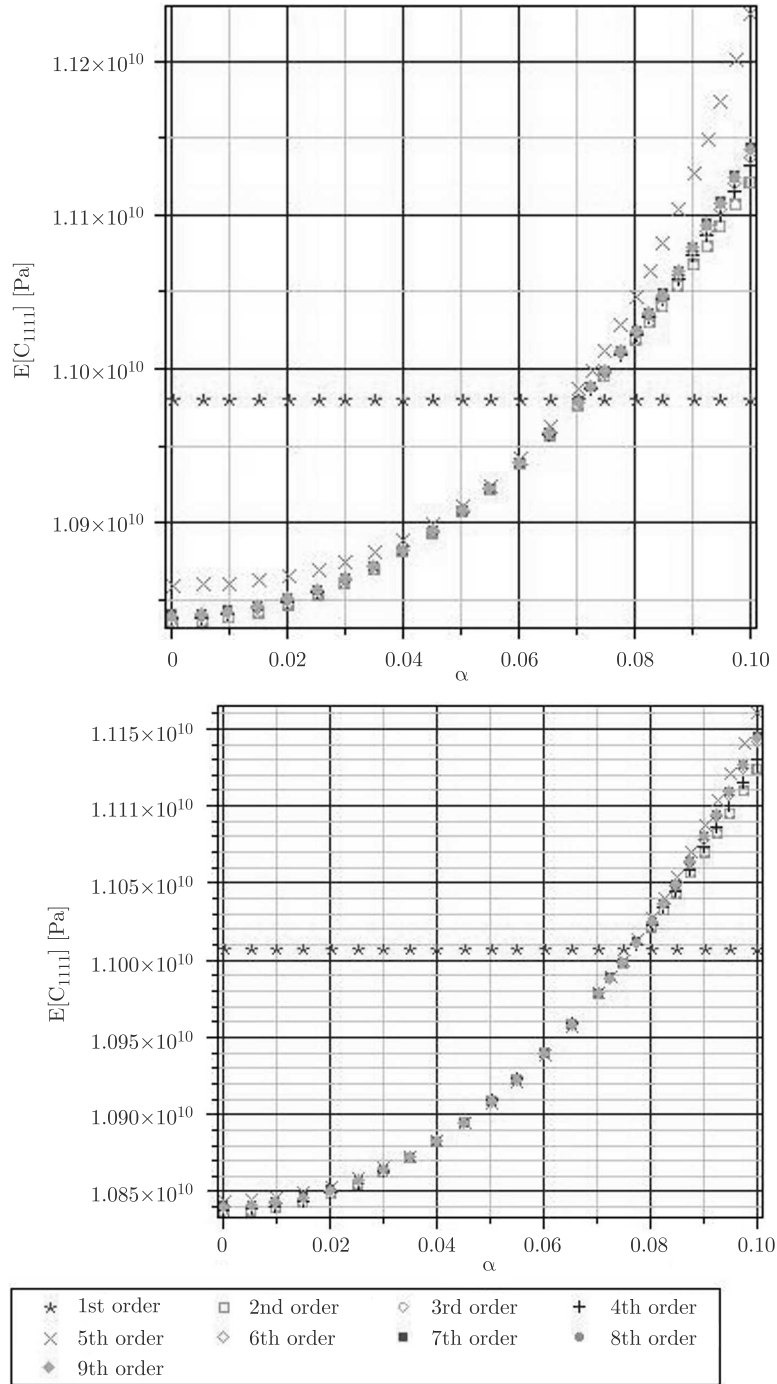


FIG. 7. The WLSM expected values  $E[C_{1111}^{(\text{eff})}(\nu_2)]$ , triangular vs. Dirac weights.

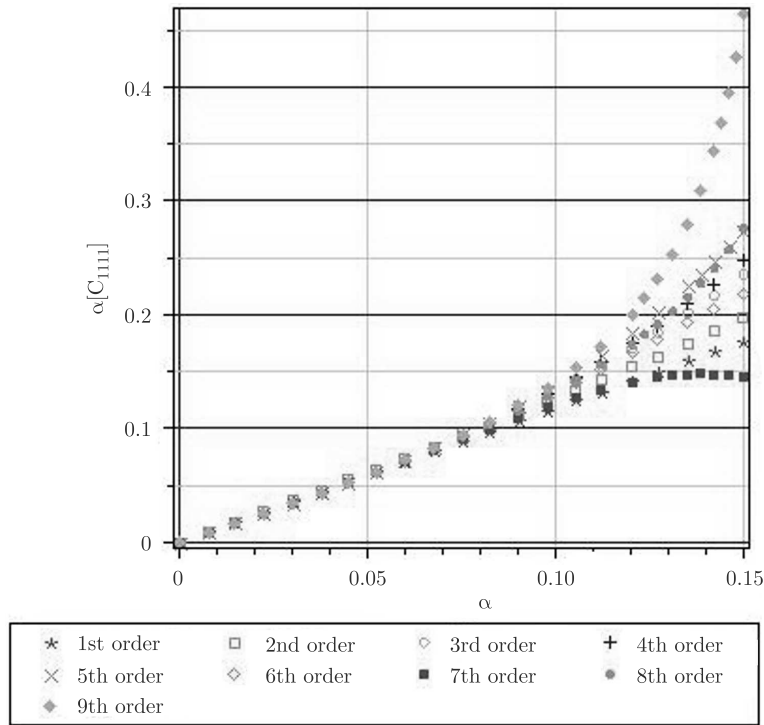


FIG. 8. The ULSM coefficients of variation  $\alpha(C_{1111}^{(eff)}(\nu_2))$ .

Figures 8 and 9 contain the coefficient of variation  $\alpha(C_{1111}^{(eff)})$  shown as the function of  $\alpha(\nu_2)$ , but now the second parameter varies in the interval  $[0.0,0.15]$  – far beyond the second-order second moment limitations. The tendency of ULSM approach to overestimate the output characteristics is quite clear also in Fig. 8, where output maximum coefficient is almost three times larger than the input one. This method returns the stable and convergent result for smaller values of the input random variable rather, like from 0.0 up to 0.1. The additional interrelations between the input and output coefficient of variation presented in both parts of Fig. 9 as the function of the response polynomial order, show that we need to exclude the first two orders from the WLSM approach results, while the remaining higher orders return the very stable values, which are very close to each other.

### 6. Concluding remarks

1. The validation test of the 1D composite structure homogenization with randomized Young’s modulus of the reinforcement, where analytical solution exists, shows a perfect agreement between probabilistic analytical determina-

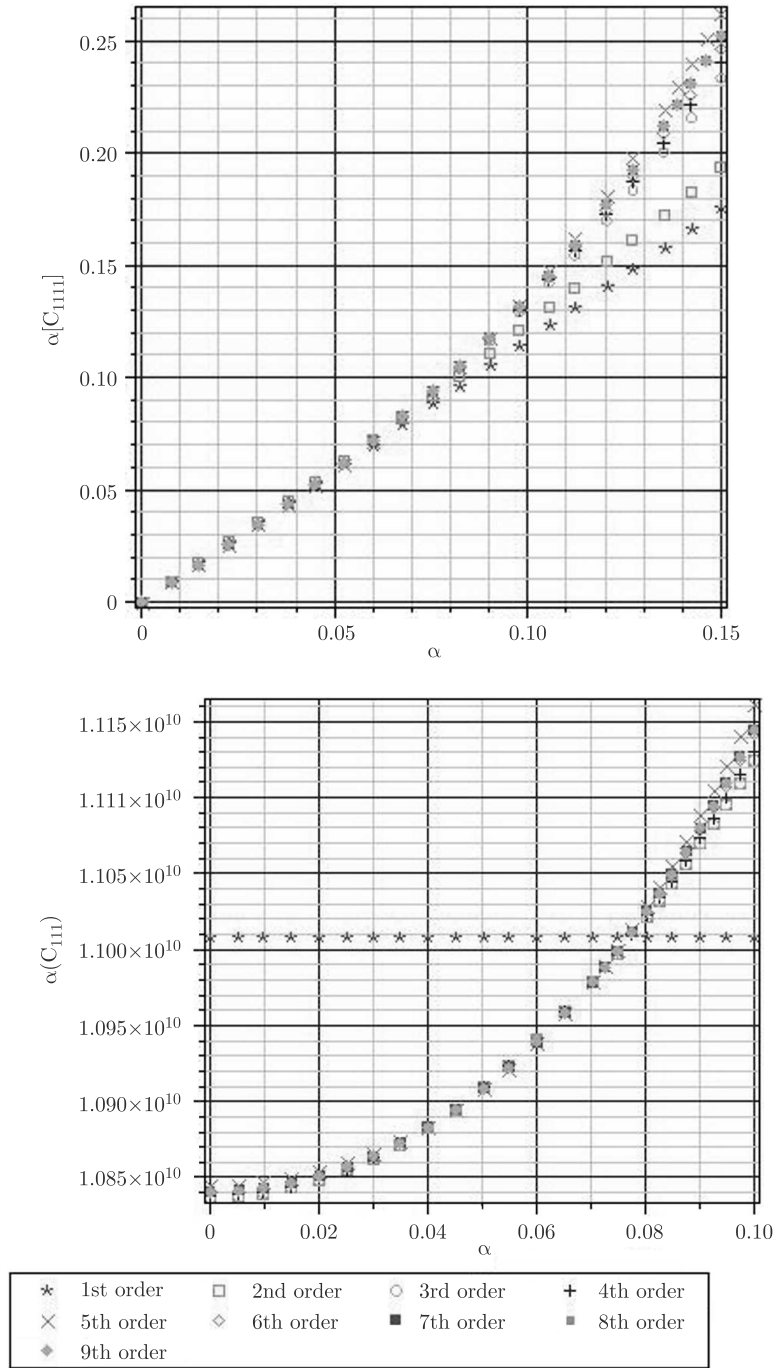


FIG. 9. The WLSM coefficients of variation  $\alpha(C_{1111}^{(\text{eff})}(\nu_2))$ , triangular vs. Dirac weights.

tion for the moments, the statistical Monte-Carlo simulation method as well as non-statistical generalized stochastic perturbation technique, applied further to homogenize the fiber-reinforced structure. The direct integration method is available thanks to the application of the computer algebra system only and, at the same time, only for the truncated Gaussian random variables. Some small numerical discrepancies are noticed for the third probabilistic moments and characteristics and they may need longer expansions than that provided in the present perturbation-based model. All computational techniques applied uniquely show that the homogenized elastic characteristics have Gaussian distributions, and that the overall computational cost of probabilistic homogenization for analytical and perturbation methods are the same.

2. The weighting procedure applied here to increase computational efficiency of the traditional Least Squares Method (LSM) appears to be very efficient, especially when the Dirac type function represents the importance of the particular trial points with the peak corresponding to the expectation of the input random variable. It essentially speeds up the probabilistic convergence of central moments of the homogenized elasticity tensor for the entire considered variability interval of the input coefficient of variation. Triangular distribution of the weights is less effective than the Dirac function in stabilization of the final probabilistic moments – we notice larger variations in the first case, especially for maximum random deviation of the input. Thanks to the application of the WLSM–SFEM with the Dirac weights, it is possible to significantly decrease the required response polynomial order from 9-th to almost the second. It should be mentioned that the computational analysis supporting those conclusions has been provided by randomization of the matrix Poisson’s ratio, where previously the Least Squares Method in the unweighted version shown the worst efficiency, the response polynomial needed to be of a very high order and the sensitivity gradients of homogenized tensor components were apparently the largest.

3. Further developments of this methodology may progress in quite different directions – one may try to increase the order of the primary deterministic perturbation included into the initial homogenization equation to calculate higher-order correctors than the first one [5]. Further comparison with the Monte-Carlo simulations, also for other types of constituents compositions (in the context of various contrasts between the expected values of material parameters), may be very helpful to calibrate the Dirac weight peaks for the expectations to have the probabilistic moments in WLSM-SFEM technique very close to the statistical estimators. Nevertheless, an extension towards inclusion of the stochastic ageing phenomena may be provided thanks to the experimentally verified time variations of the expectations and standard deviations of materials characteristics of the particular components. A certain open question is further

application of this homogenization procedure to the practical reliability assessment for various frequently exploited engineering composites. Computational implementation of the nonlinear constitutive relations and, especially, the corresponding homogenization method, would not be a straightforward extension of the approach presented in the paper, although the presence of stochastic interface defects [7, 9] or some cohesion at the interface [12] would be decisively simpler.

## 7. Acknowledgment

The author would like to gratefully acknowledge the financial support of the Polish Ministry of Science and Higher Education under the Research Grant No NN 519-386-636.

## References

1. J.S. BENDAT, A.G. PIERSOL, *Random Data: Analysis and Measurement Procedures*, Wiley, New York 1971.
2. A. BENSOUSSAN, J.L. LIONS, G. PAPANICOLAOU, *Asymptotic Analysis for Periodic Structures*, North-Holland, Amsterdam 1978.
3. R.M. CHRISTENSEN, *Mechanics of Composite Materials*, Wiley, New York 1979.
4. M.E. CRUZ, A.T. PATERA, *A parallel Monte-Carlo finite element procedure for the analysis of multicomponent media*, Int. J. Num. Meth. Engrg. **38**, 1087-1121, 1995.
5. J. FISH, W. CHEN, *Higher order homogenization of initial boundary value problem*, J. Engrg. Mech., **127**, 12, 1223-1230, 2001.
6. D. JEULIN, M. OSTOJA-STARZEWSKI, [Eds.], *Mechanics of Random and Multiscale Structures*, CISM Courses and Lectures No. 430, Springer, Wien, New York 2001.
7. M. KAMIŃSKI, *Computational Mechanics of Composite Materials*, Springer, London, New York 2005.
8. M. KAMIŃSKI, *Sensitivity and randomness in homogenization of periodic fiber-reinforced composites via the response function method*, Int. J. Sol. Struct., **46**, 923-937, 2009.
9. M. KAMIŃSKI, M. KLEIBER, *Numerical homogenization of n-component composites including stochastic interface defects*, Int. J. Num. Meth. Engrg., **47**, 1001-1027, 2000.
10. M. KAMIŃSKI, B.A. SCHREFLER, *Probabilistic effective characteristics of cables for superconducting coils*, Comput. Meth. Appl. Mech. Engrg., **188**, 1-3, 1-16, 2000.
11. A.L. KALAMKAROV, A.G. KOLPAKOV, *Analysis, Design and Optimization of Composite Structures*, Wiley, 1997.
12. F. LENÉ, D. LEGUILLON, *Homogenized constitutive law for a partially cohesive composite material*, Int. J. Sol. Struct., **18**, 443-458, 1982.

- 
13. S. SAKATA, F. ASHIDA, T. KOJIMA, M. ZAKO, *Three-dimensional stochastic analysis using a perturbation-based homogenization method for elastic properties of composite material considering microscopic uncertainty*, Int. J. Sol. & Struct., **45**, 894–907, 2007.
  14. E. SANCHEZ-PALENCIA, *Non-Homogeneous Media and Vibration Theory*, Springer, 1980.
  15. K. TERADA, T. MIURA, N. KIKUCHI, *Digital image-based modeling applied to the homogenization analysis of composite materials*, Comput. Mech., **20**, 331–346, 1997.
  16. M. TOOTKABONI, L. GRAHAM-BRADY, *A multiscale spectral stochastic method for homogenization of multi-phase periodic composites with random material properties*, Int. J. Num. Meth. Engrg., **83**, 59–90, 2010.

Received November 29, 2010; revised version March 26, 2011.

---